Journal of Biomedical Optics

SPIEDigitalLibrary.org/jbo

Physical and mathematical modeling of antimicrobial photodynamic therapy

Lisa Bürgermeister
Fernando Romero López
Wolfgang Schulz

SPIE

Journal of Biomedical Optics 19(7), 071411 (July 2014)

Physical and mathematical modeling of antimicrobial photodynamic therapy

Lisa Bürgermeister,[a,*] Fernando Romero López,[a] and Wolfgang Schulz[a]
[a]Fraunhofer Institute for Laser Technology, Steinbachstr. 15, Aachen D-52074, Germany

Abstract. Antimicrobial photodynamic therapy (aPDT) is a promising method to treat local bacterial infections. The therapy is painless and does not cause bacterial resistances. However, there are gaps in understanding the dynamics of the processes, especially in periodontal treatment. This work describes the advances in fundamental physical and mathematical modeling of aPDT used for interpretation of experimental evidence. The result is a two-dimensional model of aPDT in a dental pocket phantom model. In this model, the propagation of laser light and the kinetics of the chemical reactions are described as coupled processes. The laser light induces the chemical processes depending on its intensity. As a consequence of the chemical processes, the local optical properties and distribution of laser light change as well as the reaction rates. The mathematical description of these coupled processes will help to develop treatment protocols and is the first step toward an inline feedback system for aPDT users. [DOI: 10.1117/1.JBO.19.7.071411]

Keywords: photodynamic therapy; reaction diffusion kinetics; radiative transfer; periodontal treatment.

Paper 130685SSRR received Sep. 20, 2013; revised manuscript received Mar. 18, 2014; accepted for publication Apr. 22, 2014; published online May 21, 2014.

1 Introduction

Antimicrobial photodynamic therapy (aPDT) is used to treat local bacterial infections, e.g., oral infections, infected wounds, or local infections with multiresistant bacteria. Our current research focuses on the improvement of the treatment of periodontitis.

Periodontitis is an infection of the periodontium caused by bacteria. It leads to the formation of a dental pocket, where the bacteria settle and which cannot be cleaned by domestic oral hygiene. If periodontitis remains untreated, it will cause the reduction of jaw bone and gum and induce loose teeth and tooth loss. 30% to 50% of European adults suffer from periodontitis, 10% of them with advanced cases.[1] The medical treatment option is cleaning the periodontium of bacteria. The sterilization of the dental pocket via aPDT is a promising method, which reduces pain and bleeding during therapy and has the potential for better results compared to conventional mechanical treatment modalities. In addition, it does not cause bacterial resistance as the treatment with antibiotics does. However, the variety of clinical trials to evaluate the therapy outcome of aPDT leads to very varying results and shows that the mechanisms of aPDT are so far not well understood and thus not well controlled. The potentials of aPDT are therefore not exploited.[1–9]

Mathematical and physical modeling of the therapy is a promising approach to understand the characteristic properties of aPDT procedure, optimize its treatment protocols, and improve the therapy outcome. Once established, the mathematical model gives the possibility of overcoming the main drawback of aPDT: the treating dentist receives no inline feedback concerning therapy progress.

The basic concepts of aPDT are known in literature.[10] We will consider the so-called type II mechanism here, which is believed to be the dominant mechanism in aPDT.[11] It consists of a photo-active agent, the so-called photosensitizer (PS), that is applied to the infected area. The molecules of the photosensitizer accumulate close to the bacteria,[12] they are activated by laser radiation in a low-power range ($\sim$ mW), then biochemical reactions occur and lead to the formation of highly reactive singlet oxygen that destroys the bacteria.

The photochemical reactions during aPDT follow the ones of photodynamic therapy (PDT) in tumor treatment, which has been investigated for several decades.[13–21] The mechanisms are visualized in Fig. 1. The PS appears in three electronic states: the ground state S_0, the excited singlet state S_1, and the triplet state T. A portion of the excited states S_1 and T decays back to the ground state and thereby emits fluorescence and phosphorescence photons. Alternatively, the triplet state T can transmit its energy to the oxygen in ground state $^3O_2$ by a collision, and thus the cytotoxic singlet oxygen $^1O_2$ is generated. The singlet oxygen $^1O_2$ acts in two possible mechanisms: it inactivates cell receptors R (cytotoxicity in Fig. 1) or degenerates photosensitizer S_0 (photobleaching in Fig. 1).

Photobleaching of other photosensitizer states (S_1, T) has also been observed,[16] but oxygen mediated bleaching of the PS ground state S_0 was found to be the dominant mechanism in PDT.[21]

For mathematical modeling of aPDT, at least three different processes need to be described: radiative transfer in periodontium, photochemical reactions leading to antimicrobial activity, and bacteria damage and diffusion processes, which are the results of gradients in concentrations after photochemical reactions.

For the description of radiative transfer in biological and thus scattering tissue, the Monte Carlo method described in detail by Wang et al.[22] is a widely used method and has already been applied to calculate the radiation distribution inside the periodontium.[23]

*Address all correspondence to: Lisa Bürgermeister, E-mail: lisa.buergermeister@ilt.fraunhofer.de

0091-3286/2014/$25.00 © 2014 SPIE

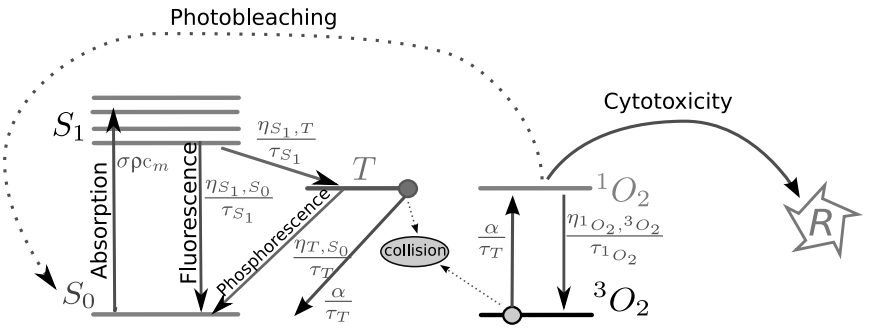

Fig. 1 Jablonski presentation of the chemical processes during PDT according to Ref. 17.

A rate equation model to describe the photochemical processes during PDT for a homogeneous distribution of concentration of reacting substances has been developed by Foster et al.[13] Taking into account an inhomogeneous light distribution, a reaction diffusion system has to be considered.[19] Hu et al.[17] included a cell repair rate of damaged cells and thereby extended Foster et al.[13] model by a constant cell repair rate for the cell receptors, which leads to a qualitative change of the properties of the solution. In order to evaluate the therapy outcome, Gkigkitzis[24] introduced a seventh rate equation for the survival fraction of cells, which is linearly dependent on the receptor concentration $[R]$.

The influence of the chemical processes (e.g., photobleaching Fig. 1) on the optical properties in the irradiated area has been investigated. In order to describe the photobleaching activity during the processes, a photobleaching rate was introduced and photobleaching was described as dependent on the local intensity.[25,26]

The above described models of the PDT processes are seen to be applicable for aPDT. The change of the optical properties due to photobleaching during aPDT and its influence on the therapy evolution is examined in this paper. Therefore, we directly couple a reaction diffusion equation system, which models the chemical processes during aPDT, with a Monte Carlo model for radiation transport.

The model described in this paper is able to simulate the processes in an experimental setup for aPDT including a phantom model of a periodontium and a homogeneous solution of bacteria and photosensitizer. This step is necessary to investigate the accuracy of our model in an easily observable environment. The main differences between the simulated and clinical situations are:

- In the model, the laser source is not moved inside the dental pocket.
- Mass transport among dental pocket, gum, and dentine is forbidden in the model.
- Bacteria, photosensitizer, and oxygen are considered to be in homogeneous solutions.

The model can be extended by those phenomena but at this state, we focus on demonstrating the influence of the change of optical properties during aPDT.

2 Numerical Model

2.1 *Mathematical Task*

The goal of the numerical model of aPDT is to determine the local temporal therapy success. The quantity used to describe the therapy success is the survival fraction $B(\vec{r},t)$ of bacteria in the dental pocket

$$B(\vec{r},t) = \sum_{i=r_{\min}}^{r_0} \mathcal{B}(i|[R](\vec{r},t)/[R]_0; r_0)$$
$$r_{\min}, r_0 \in \mathbb{N}, \vec{r} \in \mathbb{R}^3, t \in [0,\infty), \quad (1)$$

where $\mathcal{B}(i|p;n)$ is the binomial distribution with parameters i, p, and n. i is the number of successful trials, p is the probability of success in one trial, n is the number of total trials, r_0 is the initial number of receptors of a living bacteria, $r_{\min}$ is the minimal number of receptors a living bacteria needs, $[R](\vec{r},t)$ is the local and temporal concentration of bacterial receptors, and $[R]_0$ is the initial value.

The receptor R is the part of the bacterial membrane that reacts with the singlet oxygen $^1O_2$. It has no biological equivalent and is introduced as a measure for biological activity. A bacteria is considered to be living as long as a certain amount $r_{\min}$ of its receptors R is active. In order to deduce any information of the aPDT success from the receptor concentration $[R]$, the number of active receptors of an individual bacteria is estimated with the binomial distribution. Only those individual bacteria that have at least $r_{\min}$ receptors still active contribute to the survival fraction B. The value $B = 0$ of the survival fraction B is the criterion to measure the therapy outcome.

Our current modeling task is a two-dimensional (2-D) model of a periodontium phantom model shown in (Fig. 2). aPDT takes place in the area of the dental pocket Ω_{aPDT} only. All the substances taking part in aPDT are homogeneously distributed at the beginning of the therapy. In the area of gingiva Ω_{ging} and the dentine Ω_{dent} only radiative transfer is considered (Fig. 2). The laser radiation is entering the calculation area with a Gaussian intensity profile at the boundaries $\Gamma_{\text{abs},1}$ or $\Gamma_{\text{abs},2}$. Any caustic of the Gaussian beam is neglected.

In order to determine the receptor concentration $[R](\vec{r},t)$ in our calculation area, we revert to the Foster et al. and Hu et al. rate equation model.[13,17] As explained there in detail, the concentrations of the three PS states $[S_0]$, $[S_1]$, and $[T]$, and the two of oxygen $[^3O_2]$ and $[^1O_2]$, change in time due to photochemical processes (absorption, fluorescence, phosphorescence and resonant collision, cytotoxicity, and photobleaching, see Fig. 1). Those processes and the change of oxygen concentration in space due to diffusion processes are expressed mathematically in Eqs. (2)–(6)

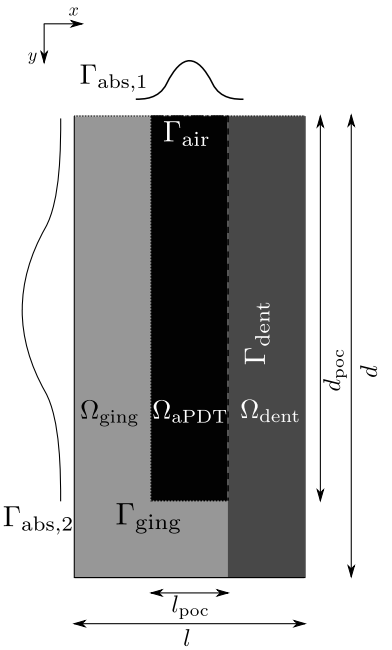

Fig. 2 Schematic representation of the calculation area. The dimensions of the area and the boundaries for diffusion processes are seen.

$$\frac{d[S_0](\vec{r},t)}{dt} = -\sigma_{\mathrm{PSa}} c\rho(\vec{r},t)[S_0](\vec{r},t) + \frac{\eta_{S_1,S_0}}{\tau_{S_1}}[S_1](\vec{r},t) + \frac{\eta_{T,S_0}}{\tau_T}[T](\vec{r},t) + \frac{\alpha}{\tau_T}[T](\vec{r},t)[^3\mathrm{O}_2](\vec{r},t) - k_{\mathrm{pb}}[^1\mathrm{O}_2](\vec{r},t)[S_0](\vec{r},t), \tag{2}$$

$$\frac{d[S_1](\vec{r},t)}{dt} = \sigma_{\mathrm{PSa}} c\rho(\vec{r},t)[S_0](\vec{r},t) - \frac{\eta_{S_1,S_0}}{\tau_{S_1}}[S_1](\vec{r},t) - \frac{\eta_{S_1,T}}{\tau_{S_1}}[S_1](\vec{r},t), \tag{3}$$

$$\frac{d[T](\vec{r},t)}{dt} = \frac{\eta_{S_1,T}}{\tau_{S_1}}[S_1](\vec{r},t) - \frac{\eta_{T,S_0}}{\tau_T}[T](\vec{r},t) - \frac{\alpha}{\tau_T}[T](\vec{r},t)[^3\mathrm{O}_2](\vec{r},t), \tag{4}$$

$$\frac{d[^3\mathrm{O}_2](\vec{r},t)}{dt} = -\frac{\alpha}{\tau_T}[T](\vec{r},t)[^3\mathrm{O}_2](\vec{r},t) + \frac{\eta_{^1\mathrm{O}_2,{}^3\mathrm{O}_2}}{\tau_{^1\mathrm{O}_2}}[^1\mathrm{O}_2](\vec{r},t) + D_{\mathrm{ox}}\nabla^2[^3\mathrm{O}_2](\vec{r},t), \tag{5}$$

$$\frac{d[^1\mathrm{O}_2](\vec{r},t)}{dt} = \frac{\alpha}{\tau_T}[T](\vec{r},t)[^3\mathrm{O}_2](\vec{r},t) - \frac{\eta_{^1\mathrm{O}_2,{}^3\mathrm{O}_2}}{\tau_{^1\mathrm{O}_2}}[^1\mathrm{O}_2](\vec{r},t) - k_{\mathrm{pb}}[^1\mathrm{O}_2](\vec{r},t)[S_0](\vec{r},t) - k_{\mathrm{cx}}[^1\mathrm{O}_2](\vec{r},t)[R](\vec{r},t) + D_{\mathrm{ox}}\nabla^2[^1\mathrm{O}_2](\vec{r},t), \tag{6}$$

where, $\rho(\vec{r},t)$ is the photon density at position $\vec{r}$ and time t, σ_{PSa} is the absorption cross section of PS, c is the speed of light in tissue, η_{S_1,S_0} is the quantum yield for the transition from the PS singlet state to the ground state, $\eta_{S_1,T}$ is the quantum yield for transition from the PS singlet state to the triplet state, η_{T,S_0} is the quantum yield for transition from the PS triplet state to the ground state, $\eta_{^1\mathrm{O}_2,{}^3\mathrm{O}_2}$ is the quantum yield for transition from the oxygen singlet state to the ground state, τ_{S_1} is the lifetime of PS in the singlet state, τ_T is the lifetime of PS in the triplet state, $\tau_{^1\mathrm{O}_2}$ is the lifetime of oxygen in the singlet state, α is the quantum yield of the energy transfer from PS in the triplet sate to oxygen in the ground state at a collision, k_{pb} is the photobleaching rate, k_{cx} is the cytotoxicity rate, and D_{ox} is the diffusion constant for oxygen in both states.

In accordance with Liu et al.,[21] we only include photobleaching of S_0 mediated by singlet oxygen $^1\mathrm{O}_2$ [see Eqs. (2) and (6)].

The calculation area for the rate equation systems (2)–(6) is Ω_{aPDT}, shown in Fig. 2. The boundary conditions for all concentrations $[X]$ are considered to be isolated, i.e., mass transport through the boundaries is forbidden, which means all the substances remain inside the calculation area Ω_{aPDT}. For oxygen in the ground state, values at the boundaries with air Γ_{air} are fixed and equal to the saturation concentration $[^3\mathrm{O}_2]_{\mathrm{sat}}$ of oxygen in water at 37°C

$$[^3\mathrm{O}_2](\vec{r},t)|_{\vec{r}\in\Gamma_{\mathrm{air}}} = [^3\mathrm{O}_2]_{\mathrm{sat}}, \tag{7}$$

$$\nabla[^3\mathrm{O}_2](\vec{r},t)|_{\vec{r}\in\Gamma_{\mathrm{ging}}} = \nabla[^3\mathrm{O}_2](\vec{r},t)|_{\vec{r}\in\Gamma_{\mathrm{dent}}} = \nabla[X](\vec{r},t)|_{\vec{r}\in\Gamma_{\mathrm{dent}}} = \nabla[X](\vec{r},t)|_{\vec{r}\in\Gamma_{\mathrm{ging}}} = \nabla[X](\vec{r},t)|_{\vec{r}\in\Gamma_{\mathrm{air}}} = 0, \tag{8}$$

and the initial conditions are

$$[S_0](\vec{r},t)|_{t=0,\vec{r}\in\Omega_{\mathrm{aPDT}}} = [S_0]_0, \tag{9}$$

$$[^3\mathrm{O}_2](\vec{r},t)|_{t=0,\vec{r}\in\Omega_{\mathrm{aPDT}}} = [^3\mathrm{O}_2]_0, \tag{10}$$

$$[S_0](\vec{r},t)|_{t=0,\vec{r}\in\Omega_{\mathrm{ging}}\cup\Omega_{\mathrm{dent}}} = [^3\mathrm{O}_2](\vec{r},t)|_{t=0,\vec{r}\in\Omega_{\mathrm{ging}}\cup\Omega_{\mathrm{dent}}} = [S_1](\vec{r},t)|_{t=0} = [T](\vec{r},t)|_{t=0} = [^1\mathrm{O}_2](\vec{r},t)|_{t=0} = 0. \tag{11}$$

The oxygen in the singlet state $^1\mathrm{O}_2$ reacts with the bacterial receptors R [Eq. (6)] and thereby inactivates them (cytotoxicity in Fig. 1). On the other hand, it has been observed that the bacteria profit from cell repair mechanisms.[27] Although the cell repair rate is not significant on the time scale of a successful aPDT treatment, it needs to be included in the model to cover cases of very slow or uncompleted aPDT progresses. In those cases, the therapy outcome is very sensitive to the cell repair rate. Thus, the concentration of receptors $[R]$ regenerates with the rate U

$$\frac{d[R](\vec{r},t)}{dt} = -k_{\mathrm{cx}}[^1\mathrm{O}_2](\vec{r},t)[R](\vec{r},t) + U([R]), \tag{12}$$

$$U([R]) = \sum_{i=r_{\min}}^{r_0} \mathcal{B}(i|[R](\vec{r},t);r_0)\cdot U'(i), \tag{13}$$

where

$$U'(r) = \begin{pmatrix} 0, & r < r_{\min} \\ a, & r_{\min} \le r < r_0 \\ 0, & r \ge r_0 \end{pmatrix}, \tag{14}$$

where, r is the receptors of an individual bacterium, r_0 is the initial number of receptors of a living bacterium, $r_{\min}$ is the minimal number of receptors of a living bacterium, and a is the constant cell repair rate.

The diffusion of bacteria, and thus receptors, is not considered in this model, since bacteria will not be totally destroyed but only devitalized. This does not lead to gradients in bacteria concentration. Diffusion of PS is not considered in Eqs. (2)–(4), because PS is bound to the bacteria membranes. The initial condition for the bacteria receptors is

$$[R](\vec{r},t)|_{t=0,\vec{r}\in\Omega_{\mathrm{aPDT}}} = [R]_0, \tag{15}$$

$$[R](\vec{r},t)|_{t=0,\vec{r}\in\Omega_{\mathrm{ging}}\cup\Omega_{\mathrm{dent}}} = 0. \tag{16}$$

The local photon density $\rho(\vec{r},t)$ is required as input in Eqs. (2) and (3) to induce the photochemical reactions and thus reduce the survival fraction $B(\vec{r},t)$.

The propagation of light, the chemical processes during aPDT, and the diffusion processes inside the treated area are coupled processes as the local radiation intensity enables the chemical reactions and depends on the local optical properties, which are strongly influenced by the concentration of PS. In addition, due to photobleaching, the local PS concentration varies. The photon density $\rho(\vec{r},t)$ is determined by

$$\rho(\vec{r},t) = \int_{2\pi} N(\vec{r},\hat{s},t)\mathrm{d}\Omega \tag{17}$$

$$\begin{aligned}\frac{1}{c}\frac{dN(\vec{r},\hat{s},t)}{dt} = &-\hat{s}\nabla N(\vec{r},\hat{s},t) - (\sigma_{\mathrm{PSa}}[S_0](\vec{r},\hat{s},t) \\ &+ \mu_{a0})N(\vec{r},\hat{s},t) - (\sigma_{\mathrm{PSs}}([S_1](\vec{r},t) + [T](\vec{r},t)) \\ &+ \mu_{s0})N(\vec{r},\hat{s},t) + (\sigma_{\mathrm{PSs}}([S_1](\vec{r},t) \\ &+ [T](\vec{r},t)) + \mu_{s0}) \int_{2\pi} p(\hat{s}',\hat{s})N(\vec{r},\hat{s}',t)\mathrm{d}\Omega',\end{aligned} \tag{18}$$

with the boundary conditions for the photon number N at the surface exposed to laser light Γ_{abs}

$$N(\vec{r},\hat{s},t)|_{\vec{r}\in\Gamma_{\mathrm{abs},1}} = N_0 \mathrm{e}^{-2x^2/w_0^2}\vec{e}_y, \tag{19}$$

$$N(\vec{r},\hat{s},t)|_{\vec{r}\in\Gamma_{\mathrm{abs},2}} = N_0 \mathrm{e}^{-2y^2/w_0^2}\vec{e}_x, \tag{20}$$

and the initial condition

$$N(\vec{r},\hat{s},t)|_{t=0} = 0, \tag{21}$$

where, $N(\vec{r},\hat{s},t)$ is the number of photons traveling at position $\vec{r}$ at time t along direction $\hat{s}$ through surface dA in solid angle $d\Omega$, N_0 is the number of photons at the center of the Gaussian beam, w_0 is the beam radius of the Gaussian beam, σ_{PSs} is the scattering cross section of PS, σ_{PSa} is the absorption cross section of PS, μ_{a0} is the absorption coefficient of other substances, μ_{s0} is the scattering coefficient of other substances, $p(\hat{s}',\hat{s})$ is the phase function for scattering from direction $\hat{s}'$ in direction $\hat{s}$, and $\vec{e}_{x/y}$ is the unity vector in x/y direction.

2.2 *Radiative Transfer*

Due to its fast time scale, the intensity distribution relaxes quickly to its temporary equilibrium and the stationary equation of radiative transfer

$$\begin{aligned}\hat{s}\nabla N(\vec{r},\hat{s},t) = &-(\sigma_{\mathrm{PSa}}[S_0](\vec{r},\hat{s},t) + \mu_{a0})N(\vec{r},\hat{s},t) \\ &- (\sigma_{\mathrm{PSs}}([S_1](\vec{r},t) + [T](\vec{r},t)) + \mu_{s0})N(\vec{r},\hat{s},t) \\ &+ (\sigma_{\mathrm{PSs}}([S_1](\vec{r},t) + [T](\vec{r},t)) + \mu_{s0}) \\ &\int_{2\pi} p(\hat{s}',\hat{s})N(\vec{r},\hat{s}',t)\mathrm{d}\Omega'\end{aligned} \tag{22}$$

is solved. To do so, we use the Monte Carlo method. Its principles are explained in the literature, e.g., Wang et al.[22] The incident intensity distribution is a Gaussian distribution represented by a density distribution of single photons at the boundary $\Gamma_{\mathrm{abs},1/2}$ of the calculation area. Using homogeneous distributed random numbers, we calculate the free path length δ of every photon and its next position of interaction. For every interaction, another random number ξ determines whether the photon is absorbed or scattered. The scattering angle θ follows a third random number, which is generated by the Henyey–Greenstein probability distribution

$$p(\cos\theta) = \frac{1-g^2}{2(1+g^2-2g\cos\theta)^{3/2}}. \tag{23}$$

This distribution was found to be accurate for biological tissues.[22] θ indicates the scattering angle and g is the anisotropy coefficient. Since the local optical properties change in the volume according to the rate equations, the photon density distribution has to be updated after every change of the PS concentration $[S_0](\vec{r},t)$. The local optical properties are stored in a grid with side lengths Δx and Δy. When a photon crosses the border between two grid cells, the covered path length is subtracted from the original path length and the rest of it is scaled in order to comply with the local optical properties in the current grid cell (Fig. 3). The photon density inside the calculation area is stored and serves as an input parameter for the rate equations at every grid cell.

2.3 *Antimicrobial Photodynamic Therapy Reaction Kinetics and Diffusion*

The system of partial differential Eqs. (2)–(6) and (12) is solved on the same 2-D grid as the Monte Carlo simulations (Fig. 3). In order to reduce calculation time, we decide to choose two different time steps for the reaction kinetics and diffusion terms. The numerical procedure is shown for the reaction diffusion equation of oxygen in its ground state $[^3O_2]$, but is analogous for the other concentrations. The total change of oxygen is

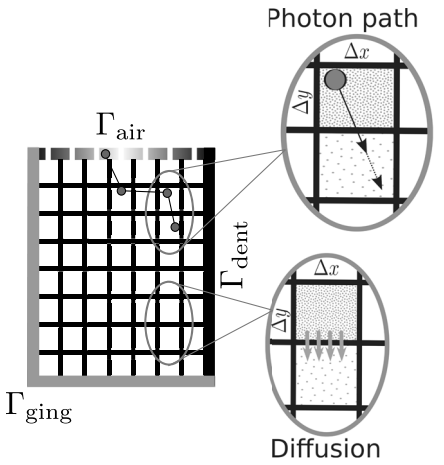

Fig. 3 Schematic representation of the dental pocket Ω_{aPDT}. The processes describing interaction between two grid cells are sketched.

$$\Delta[^3O_2] = \int_{t_n}^{t_n+\Delta t} \frac{\partial[^3O_2]}{\partial t}\, dt + \int_{t_n}^{t_n+\Delta t} D_{\text{ox}} \nabla^2 [^3O_2] \mathrm{d}t. \quad (24)$$

The diffusion term $D_{\text{ox}}\nabla^2[^3O_2]$ is evaluated at the time step t_n using the finite-difference method (Fig. 3). The result is used as a constant diffusion term in the rate equation for oxygen. The rate equation is solved by the MATLAB solver ode23t until the time $t_{n+1} = t_n + \Delta t$ is reached. At the time t_{n+1}, the diffusion term is evaluated as a first prediction. The rate equations are solved again using a linear interpolation between the diffusion terms at t_n and t_{n+1} and more accurate results of the rate equations are received.

3 Results and Discussions

We analyzed our model for one parameter seed point as seen in Table 1. The laser parameters are chosen according to typical values in clinical trials and practice. Typical exposure times in clinical practice are 30 s of continuous wave (CW) irradiation per spot. Our simulations are performed for at least 40 s CW irradiation. The parameters are taken from the literature or, if not available there, a reasonable value is chosen. Any usage of parameters different from Table 1 is declared explicitly. The conclusions made in this paper have to be seen as qualitative results, which can be observed and compared to experimental results. We show that the physical and mathematical modeling of aPDT leads to a better understanding of the therapy. In order to obtain quantitative results and predictions for medical treatment, parameters have to be adjusted and the model has to be refined.

3.1 *Homogeneous Model*

In order to gain an understanding of how the concentrations in the irradiated area evolve in time, a zero-dimensional model is solved as a first step. The solution of this point system is equivalent to the solution of a system extended in space with homogeneously distributed initial conditions and processing parameters. In such a system, both transport processes and position play no role for the evolution of concentrations. The evolution of the concentrations in time in such a point system is shown for two sets of initial conditions in Figs. 4 and 5. The therapy success is expressed in the survival fraction B of the bacteria. The therapy is successful if the survival fraction B is reduced to zero during the irradiation time, which is the case in Fig. 4. After the receptors R are significantly reduced, some decrease in PS and oxygen concentration can be noticed. This decrease is the result of the oxidation reaction between PS (S_0) and oxygen ($^1O_2$), called photobleaching (see Fig. 1). Photobleaching leads to a reduction of the PS concentration and is followed by higher penetration of laser light into the irradiated area. In the double logarithmic presentation, the comparatively steep decay of receptors R and survival fraction B is very striking. The therapy success is achieved only after a certain irradiation time with a constant intensity. This behavior of a minimum threshold dose for laser radiation has been observed in PDT for cancer treatment experimentally[31] and we expect to find it in experiments for aPDT as well.

In addition, some significance of the ratio of the initial value of oxygen concentration and receptor concentration $[^3O_2]_0/[R]_0$ can be seen. In Fig. 4, this ratio is $[^3O_2]_0/[R]_0 = 1.2$ and the therapy success is achieved after 12 s of irradiation. With a too little initial value for oxygen concentration ($[^3O_2]_0/[R]_0 = 0.8$ in Fig. 5), the therapy is not successful ($B > 0$) after 100 s. Instead, the reduction of the survival fraction B is limited because the oxygen concentration is reduced to zero before enough bacterial receptors are oxidized. The constant photon density is $\rho = 2 \cdot 10^6$ cm^{-3} in both figures. All the other parameters correspond to the parameter seed point, listed in Table 1.

Using scatterplots, we analyzed the therapy outcome $B = 0$ after 30 s of irradiation. We found that the initial value of the oxygen concentration $[^3O_2]_0$ is the most sensitive parameter of the therapy outcome $B = 0$ at our seed point (Table 1). Analyzing the homogeneous model around its parameter seed point, we saw that the ratio between theb initial value of oxygen concentration and receptor concentration $[^3O_2]_0/[R]_0$ has to be at least 1 to reduce the receptor concentration significantly. Therefore, we use $[^3O_2]_0/[R]_0 = 1.2$ as this ratio for all our calculations. The scatterplot for the survival fraction $B(30\text{ s})$ after 30 s of irradiation is shown in Fig. 6. We learn from Fig. 6 that successful aPDT is not possible without the presence of oxygen. If enough oxygen is available at the beginning of the treatment, the reduction of the survival fraction B to 0 depends on other parameters. Therefore, aPDT has to be planned carefully with a deep understanding of the underlying physical and chemical processes.

3.2 *Therapy Progress*

The characteristic result of our model is shown in Fig. 7. The irradiated and thus successfully ($B = 0$) treated area is growing in time. The calculation is performed with the parameters given in Table 1. For the survival fraction, no transition is seen between $B = 1$ and $B = 0$. This is explained by the steep reduction of B already seen in the homogeneous model (Fig. 4). At the positions $\vec{r}$, where the survival fraction of bacteria B is reduced to virtually zero, photobleaching occurs and photons travel further inside the volume. Therefore, additional to the time required by the reaction kinetics to reduce the survival fraction of bacteria B (12 s in Fig. 4), the time that photons need to reach the position $\vec{r}$ has to be considered for the therapy. This is visualized in Fig. 8 for the same calculations. Therefore, the evolution of survival fractions B at three different heights of the dental pocket is seen. As expected, the survival fraction is much more quickly reduced on the top of the dental pocket Ω_{aPDT} than at its bottom. There, after some seconds only, a sufficient photon density is reached.

Table 1 Parameter seed point.

Symbol	Name
$r_0 = 100$	Initial number of receptors of a living bacteria
$r_{min} = 0.1 r_0$	Minimal number of receptors a living bacteria needs
$[^3O_2]_0/[R]_0 = 1.2$	Initial value of triplet oxygen concentration
$[^1O_2]_0/[R]_0 = 0$	Initial value of singlet oxygen concentration
$[^3O_2]_{sat}/[R]_0 = 0.5$	Saturation concentration of oxygen in water
$[S_0]_0/[R]_0 = 0.2$	Initial value of PS in ground state[16]
$[S_1]_0/[R]_0 = 0$	Initial value of PS in singlet state
$[T]_0/[R]_0 = 0$	Initial value of PS in triplet state
$\sigma_{PSa} = 1.7 \cdot 10^{-17}$ cm^2	Absorption cross section of PS[16]
$\eta_{S_1,S_0} = 0.2$	Quantum yield for transition from PS singlet state to ground state[17]
$\eta_{S_1,T} = 0.8$	Quantum yield for transition from PS singlet state to triplet state[17]
$\eta_{T,S_0} = 0.3$	Quantum yield for transition from PS triplet state to ground state[17]
$\eta^1O_2,^3O_2 = 0.3$	Quantum yield for transition from oxygen singlet state to ground state[17]
$\tau_{S_1} = 10$ ns	Lifetime of PS in singlet state[28]
$\tau_T = 0.3$ ms	Lifetime of PS in triplet state[29]
$\tau^1O_2 = 30$ ns	Lifetime of oxygen in singlet state[29]
$\alpha = 10^{-17}$ cm^3	Quantum yield of energy transfer from PS in triplet sate to oxygen in ground state at a collision[13]
$a = 2.6 \cdot 10^{12}$ cm^{-3} s^{-1}	Constant cell repair rate[17]
$k_{pb} = 2 \cdot 10^{-10}$ cm^3/s	Photobleaching rate[30]
$k_{cx} = 2 \cdot 10^{-9}$ cm^3/s	Cytotoxicity rate[30]
$D_{ox} = 10^{-5}$ cm^2/s	Diffusion constant for oxygen in both states in water
$c = 2.17 \cdot 10^{10}$ cm/s	Speed of light in tissue[17]
$\rho_0 = 1.84 \cdot 10^6$ cm^{-3}	Maximum photon density in the center of the Gaussian beam
$w_0 = 0.1$ cm	Beam radius of the Gaussian beam
$\lambda = 630$ nm	Used wavelength[17]
$\sigma_{PSs} = 1.7 \cdot 10^{-17}$ cm^2	Scattering cross section of PS[16]
$\mu_{a0,ging} = 0.3$ cm^{-1}	Absorption coefficient of gingiva[23]
$\mu_{a0,dent} = 3$ cm^{-1}	Absorption coefficient of dentine[23]
$\mu_{a0,poc} = 30$ cm^{-1}	Absorption coefficient in dental pocket
$\mu_{s0,ging} = 150$ cm^{-1}	Scattering coefficient of gingiva[23]
$\mu_{s0,dent} = 260$ cm^{-1}	Scattering coefficient of dentine[23]
$\mu_{s0,poc} = 12000$ cm^{-1}	Scattering coefficient in dental pocket
$g_{ging} = 0.9$	Anisotropy factor of gingiva[23]
$g_{dent} = 0.9$	Anisotropy factor of dentine[23]

Table 1 (*Continued*).

Symbol	Name
$g_{poc} = 0.9$	Anisotropy factor in dental pocket[22]
$d_{poc} = 10$ mm	Depth of the dental pocket
$d = 12$ mm	Depth of the calculation area
$l_{poc} = 2$ mm	Length of the dental pocket
$l = 6$ mm	Length of the calculation area

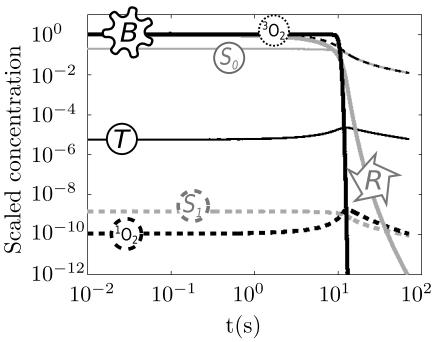

Fig. 4 Solution of the rate Eqs. (2)–(6) and (12) to describe the reaction kinetics for homogeneous distribution of initial values and a photon density constant in time and space. The initial value of oxygen concentration is $[^3O_2]_0/[R]_0 = 1.2$. The constant photon density is $\rho = 2 \cdot 10^6$ cm^{-3}. The other parameters are taken from Table 1.

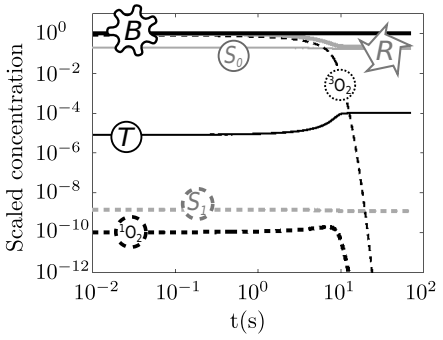

Fig. 5 Solution of the rate Eqs. (2)–(6) and (12) to describe the reaction kinetics for homogeneous distribution of initial values and a photon density constant in time and space. The initial value of oxygen concentration is $[^3O_2]_0/[R]_0 = 0.8$. The constant photon density is $\rho = 2 \cdot 10^6$ cm^{-3}. The other parameters are taken from Table 1.

Photobleaching and its influence on the optical properties in tissue have been examined experimentally and theoretically for PDT in the treatment of tumors.[18,32] In these studies, fluorescence signals of PS have been detected over time. Their dependence on the applicated laser dose supports our idea of increasing the successfully treated area.

In order to compare different settings of parameters, we introduce the quantities successfully treated area $A_{success}$

$$A_{success} = \{\vec{r} \in \Omega_{aPDT} | B(\vec{r}) = 0\}, \tag{25}$$

and total area A_0. We run our simulation for different sets of initial conditions for 120 s and evaluate the successfully treated

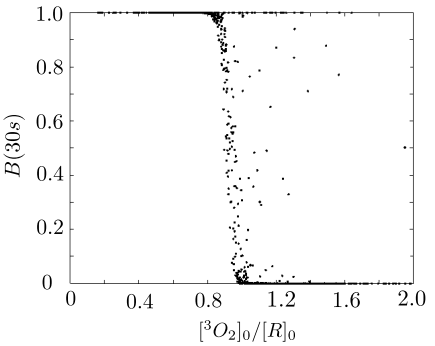

Fig. 6 Sensitivity of the survival fraction $B(30\text{ s})$ after 30 s of irradiation on the initial value of oxygen concentration $[^3O_2]_0/[R]_0$. The simulation results are obtained solving the homogeneous model for the aPDT reaction kinetics. The parameters are varied randomly around the seed point in Table 1. The photon density is varied around the value $\rho_0 = 2 \cdot 10^6$ cm^{-3}.

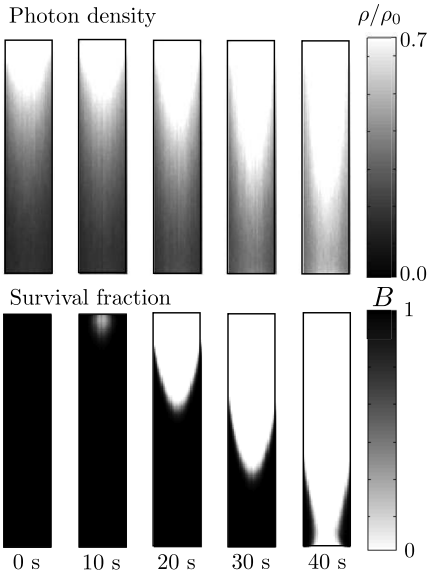

Fig. 7 Photon density $\rho(\vec{r}, t)$ and survival fraction $B(\vec{r}, t)$ at five points in time inside the dental pocket Ω_{aPDT}. The parameters for the calculation are given in Table 1.

area. The result is shown in Fig. 9. The initial conditions different from the parameter seed point (Table 1) are labeled in the graph. As already seen in the scatterplot in Fig. 6, the initial value of the oxygen concentration $[^3O_2]_0$ is the most sensitive parameter. After 120 s, the curve with an initial value of oxygen concentration $[^3O_2]_0/[R]_0 = 0.8$ shows the smallest successfully treated

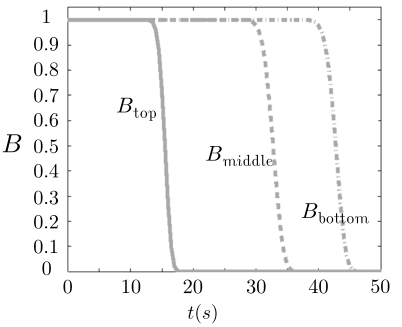

Fig. 8 Survival fraction of bacteria $B(\vec{r}, t)$ at three different heights of the dental pocket. The computation parameters are given in Table 1.

area. Due to diffusion of oxygen from the boundary to air Γ_{air} into the calculation area Ω_{aPDT} (see Fig. 3), a region with enough oxygen concentration is achieved and a small area is treated successfully. This area would be repopulated by bacteria some time after the treatment.

Our simulation shows a faster aPDT success for the PS initial concentration of $[S_0]_0/[R]_0 = 0.2$ than for the higher $[S_0]_0/[R]_0 = 1$ and the lower $[S_0]_0/[R]_0 = 0.02$ value. The lower PS initial concentration $[S_0]_0/[R]_0 = 0.02$ is not high enough to produce the necessary amount of singlet oxygen $^1O_2$ earlier, and the evolution of all the concentrations is slow. For the higher PS initial concentration $[S_0]_0/[R]_0 = 1$, a phenomenon known as self-shielding occurs. The PS concentration $[S_0]$ is so high that the light does not penetrate deep into the irradiated volume and the concentration of oxygen $[^3O_2]$ is not high enough to support the process with photobleaching. Once the oxygen $[^3O_2]$ is fully depleted, photobleaching stops and the successfully treated area A_{success} does not increase further. The photon density $\rho(\vec{r}, 120\text{ s})$, the concentration of PS $[S_0](\vec{r}, 120\text{ s})$, and the concentration of oxygen $[^3O_2](\vec{r}, 120\text{ s})$ after 120 s are shown for this set of initial condions ($[S_0]_0/[R]_0 = 1$) in Fig. 10. The oxygen concentration $[^3O_2](\vec{r}, 120\text{ s})$ is reduced to 0 in the upper part of the dental pocket Ω_{aPDT}, but the PS concentration $[S_0](\vec{r}, 120\text{ s})$ is not drastically reduced in this area. Only close to the border to air Γ_{air} is the PS concentration $[S_0](\vec{r}, 120\text{ s})$ reduced to 0. This is enabled by the diffusion of oxygen from the air into the dental pocket Ω_{aPDT}. In experiments, self-shielding of too high a PS concentration has been observed for cancer therapy.[33] The qualitative behavior of our model is supported by these experiments.

The impact of coupling radiative transfer and the ongoing rate equations can be seen in Fig. 11. We compared the

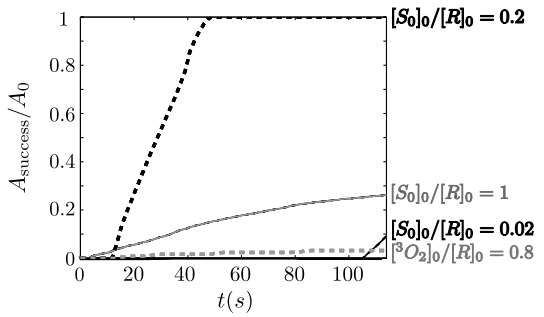

Fig. 9 Ratio of successfully treated and total area A_{success}/A_0 evolving in time for four different sets of initial conditions. The initial conditions different from the parameter seed point (Table 1) are labeled in the graph.

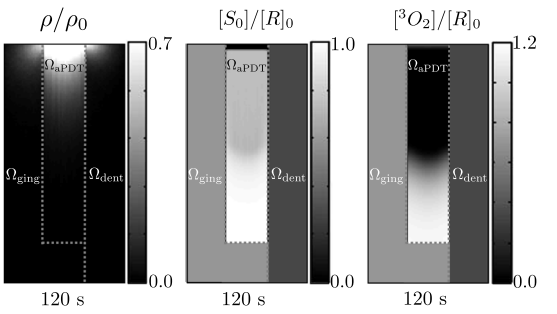

Fig. 10 Photon density $\rho(\vec{r}, 120\text{ s})$, the concentration of PS $[S_0](\vec{r}, 120\text{ s})$, and the concentration of oxygen $[^3O_2](\vec{r}, 120\text{ s})$ after 120 s of irradiation. The PS initial condition is $[S_0]_0/[R]_0 = 1$. All the other computation parameters are given in Table 1.

successfully treated area A_{success}/A_0 of our model with continuously updated optical parameters to a model with constant optical parameters. The first Monte Carlo picture served as input for the spatially distributed photon density in the case of constant optical properties. The time when the models show a successfully treated area $A_{\text{success}}/A_0 > 0$ different from zero is the same for both models. During this period, the concentrations change slightly and therefore an update of the optical properties in the irradiated area and thus of the photon density distribution is not necessary. Beyond this point in time, the successfully treated area A_{success}/A_0 increases faster for our model with updated optical properties than for the calculation with the constant light distribution. For our model, the successfully treated area A_{success}/A_0 increases nearly linearly in time for the first 38 s. Afterward, the laser radiation reaches the gingiva Ω_{ging} below the dental pocket Ω_{aPDT}. A high percentage of the photons reaching this area Ω_{ging} is scattered back into the dental pocket Ω_{aPDT} and accelerates the aPDT there. Thereby, the steep increase after approximately 40 s in Fig. 11 is explained. After 47 s of irradiation, aPDT was successful in the whole dental pocket Ω_{aPDT}.

In order to give an insight into the evolution of the other quantities, the photon density ρ, the survival fraction B, and the concentrations of the three PS states, the two oxygen states, and the receptors are shown in Fig. 12 after 40 s of irradiation from the top. (Movie 1 for 50 s of irradiation in online version).

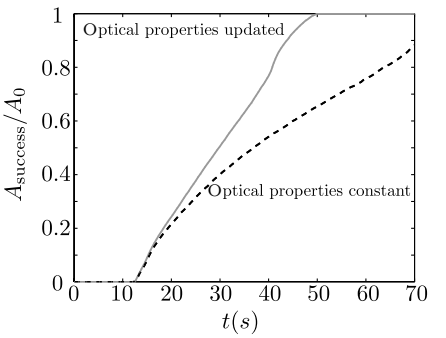

Fig. 11 Ratio of successfully treated and total area A_{success}/A_0 evolving in time for our model presented here with continuously updated optical properties and for the reaction diffusion model with a temporal constant photon density $\rho(\vec{r})$. The result of the first Monte Carlo run is used as this constant photon density $\rho(\vec{r})$. The computation parameters are given in Table 1.

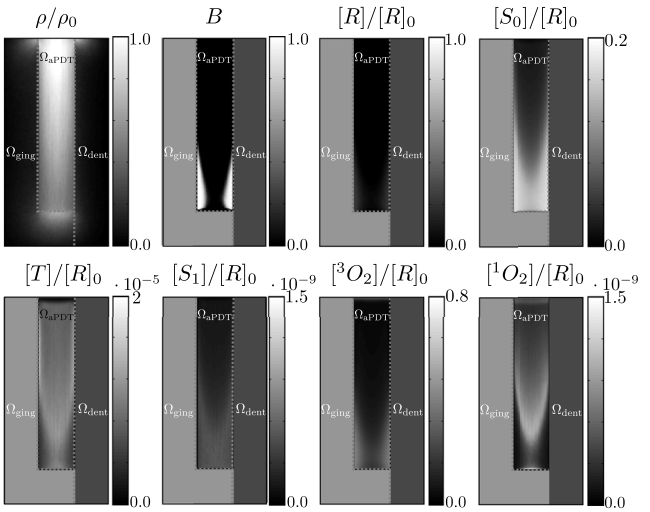

Fig. 12 Simulation of aPDT in a dental pocket with irradiation from top for 40 s. The photon density ρ, the survival fraction B, and the concentrations of the three PS states, the two oxygen states, and the receptors are displayed. The parameters are taken from Table 1. (Movie 1 (MOV 2.26 MB) [URL: http://dx.doi.org/10.1117/1.JBO.19.7.071411.1] for 50 s of irradiation in online version).

3.3 *Treatment Protocols*

In this paper, we present the simulated therapy progress for two paradigmatic treatment protocols. In Figs. 13 and 14, the therapy progress for irradiation from the top of the dental pocket $\Gamma_{\text{abs},1}$ can be seen. The used parameters are given in Table 1. In Fig. 13, the photon density $\rho(\vec{r},t)$ in the calculation area is shown at the beginning of irradiation (left) and after 40 s of irradiation (right). The survival fraction of bacteria $B(\vec{r},40\text{ s})$ after 40 s of irradiation is shown in Fig. 14.

Simulations of trans gingival irradiation from the side via $\Gamma_{\text{abs},2}$ are performed with a wider beam radius of $w_0 = 4$ mm. The rest of the set of parameters is given in Table 1. The results for the photon density $\rho(\vec{r},t)$ after 0 s (left) and 80 s (right) are shown in Fig. 15. As we increased the laser radius compared to the radiation from the top via $\Gamma_{\text{abs},1}$, but left the maximum intensity the same, the absorbed laser power is increased for the irradiation from the side. Nevertheless, after 40 s and even after 80 s of irradiation, the dental pocket Ω_{aPDT} is not totally treated successfully. In Fig. 16, the survival fraction $B(\vec{r},80\text{ s})$ is shown after 80 s of irradiation. By this time, some area of the dental

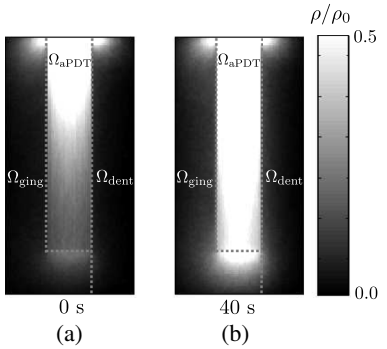

Fig. 13 Simulation of aPDT in a dental pocket with irradiation from top. (a) photon density $\rho(\vec{r},0\text{ s})$ after 0 s of irradiation. (b) photon density $\rho(\vec{r},40\text{ s})$ after 40 s of irradiation. The parameters are taken from Table 1.

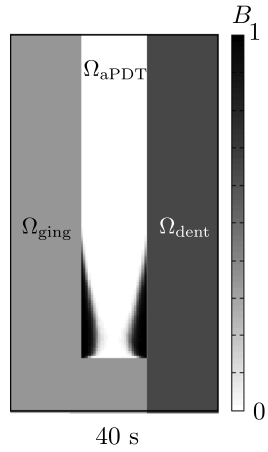

Fig. 14 Simulation of aPDT in a dental pocket with irradiation from top. Survival fraction $B(\vec{r},40\text{ s})$ after 40 s of irradiation. The parameters are taken from Table 1.

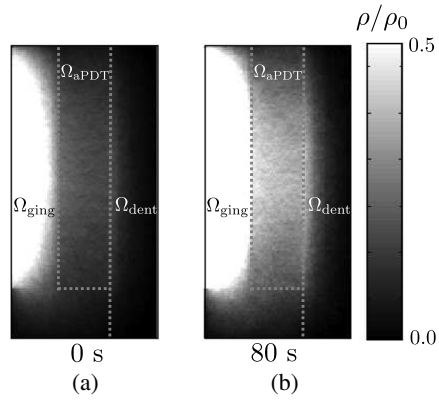

Fig. 15 Simulation of aPDT in a dental pocket with trans gingival irradiation from left side. (a) photon density $\rho(\vec{r},0\text{ s})$ after 0 s of irradiation. (b) photon density $\rho(\vec{r},80\text{ s})$ after 80 s of irradiation. The parameters are taken from Table 1.

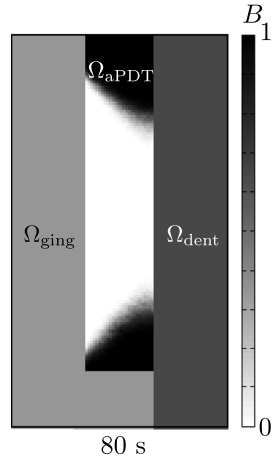

Fig. 16 Simulation of aPDT in a dental pocket with transgingival irradiation from left side. Survival fraction $B(\vec{r},80\text{ s})$ of bacteria after 80 s of irradiation. The laser radius is $w_0 = 4$ mm. The other parameters are taken from Table 1.

pocket has been treated successfully. Obviously, the protocol for the transgingival treatment has to be planned carefully under the criteria that gingiva is not hurt by the laser irradiation, but the dental pocket is treated completely.

4 Conclusion

Our results show that physical and mathematical modeling of aPDT is possible and useful for interpretation of experimental evidence. Groundbreaking results from research in cancer therapy (PDT) like spatially distributed photobleaching, threshold doses, oxygen dependencies, and self-shielding are significant in aPDT as well and can be already qualitatively reproduced by the model presented here. The current model contains some simplifications (e.g., boundary conditions) and has to be improved, but those improvements will be model refinements and will not change the basic concept presented here.

Although our simulation is performed only for one parameter seed point and some of the parameters vary on a large scale among patients, it can explain why the therapy outcomes have turned out to be so uncertain in clinical trials. In the marginal parts of the calculation area, the processes take place more slowly. Therefore, with a short time of treatment there is a high probability of bacteria surviving there, and those will recolonize later in the whole dental pocket.

Our further goal is to use modeling and simulation for optimizing aPDT in the treatment of periodontitis and designing treatment protocols. Therefore, we currently investigate the qualitative structures and properties of our model like the sensitivity concerning the indiviual parameters, aiming to efficiently continue our research.

For future research on aPDT in the treatment of periodontitis, we suggest closing the gap between *in vitro* experiments and *in vivo* animal or clinical studies. This model can be used to design an experimental *in vitro* setup closer to the clinical situation than current *in vitro* studies.

References

1. P. Meisel and T. Kocher, "Photodynamic therapy for periodontal diseases: state of the art," *J. Photochem. Photobiol. B, Biol.* **79**(2), 159–170 (2005).
2. B. W. Sigusch et al., "Eficacy of photodynamic therapy on inflammatory signs and two selected periodontopathogenic species in a beagle dog model," *J. Periodontol.*, **76**(7), 1100–1105 (2005).
3. T. Qadri et al., "The short-term effects of low-level lasers as adjunct therapy in the treatment of periodontal inflammation," *J. Clini. Periodontol.* **32**(7), 714–719 (2005).
4. R. Polansky et al., "Clinical effectiveness of photodynamic therapy in the treatment of periodontitis," *J. Clini. Periodontol.* **36**(7), 575–580 (2009).
5. R. R. de Oliveira et al., "Antimicrobial photodynamic therapy in the non-surgical treatment of aggressive periodontitis: a preliminary randomized controlled clinical study," *J. Periodontol.* **78**(6), 965–973 (2007).
6. N. Kömerik et al., "In vivo killing of porphyromonas gingivalis by toluidine blue-mediated photosensitization in an animal model," *Antimicrob. Agents Chemother.* **47**(3), 932–940 (2003).
7. O. Dörtbudak et al., "Lethal photosensitization for decontamination of implant surfaces in the treatment of peri-implantitis," *Clini. Oral Implant. Res.* **12**(2), 104–108 (2001).
8. N. Christodoulides et al., "Photodynamic therapy as an adjunct to non-surgical periodontal treatment: a randomized, controlled clinical trial," *J. Periodontol.* **79**(9), 1638–1644 (2008).
9. M. Lulic et al., "One-year outcomes of repeated adjunctive photodynamic therapy during periodontal maintenance: a proof-of-principle randomized-controlled clinical trial," *J. Clini. Periodontol.* **36**(8), 661–666 (2009).
10. Z. Malik, J. Hanania, and Y. Nitzan, "New trends in photobiology bactericidal effects of photoactivated porphyrins: an alternative approach to antimicrobial drugs," *J. Photochem. Photobiol. B, Biol.* **5**(3–4), 281–293 (1990).
11. W. M. Sharman, C. M. Allen, and J. E. van Lier, "Photodynamic therapeutics: basic principles and clinical applications," *Drug Discov. Today* **4**(11), 507–517 (1999).
12. G. Jori et al., "Photodynamic therapy in the treatment of microbial infections: Basic principles and perspective applications," *Laser. Surg. Med.* **38**(5), 468–481 (2006).
13. Th. H. Foster et al., "Oxygen consumption and diffusion effects in photodynamic therapy," *Radit. Res.* **126**(3), 296–303 (1991).
14. M. Ochsner, "Photophysical and photobiological processes in the photodynamic therapy of tumours," *J. Photochem. Photobiol. B, Biol.* **39**(1), 1–18 (1997).
15. T. J. Dougherty et al., "Review: photodynamic therapy," *J. Natl. Cancer Inst.* **90**(12), 889–904 (1998).
16. J. C. Finlay et al., "Photobleaching kinetics of photofrin in vivo and in multicell tumour spheroids indicate two simultaneous bleaching mechanisms," *Phys. Med. Biol.* **49**(21), 4837–4860 (2004).
17. X. Hu et al., "Modeling of a type II photofrin-mediated photodynamic therapy process in a heterogeneous tissue phantom," *Photochem. Photobiol.* **81**(6), 1460–1468 (2005).
18. J. S. Dysart, G. Singh, and M. S. Patterson, "Calculation of singlet oxygen dose from photosensitizer fluorescence and photobleaching during mTHPC photodynamic therapy of MLL cells," *Photochem. Photobiol.* **81**(1), 196–205 (2005).
19. K. Wang, S. Mitra, and Th. H. Foster, "A comprehensive mathematical model of microscopic dose deposition in photodynamic therapy," *Med. Phys.* **34**, 282 (2007).
20. K. Svanberg et al., "Photodynamic therapy: superficial and interstitial illumination," *J. Biomed. Opt.* **15**(4), 041502 (2010).
21. B. Liu, Th. J. Farrell, and M. S. Patterson, "A dynamic model for ALA-PDT of skin: simulation of temporal and spatial distributions of ground-state oxygen, photosensitizer and singlet oxygen," *Phys. Med. Biol.* **55**(19), 5913–5932 (2010).
22. L. Wang, S. L. Jacques, and L. Zheng, "MCML–Monte Carlo modeling of light transport in multi-layered tissues," *Comput. Meth. Prog. Biomed.* **47**(2), 131–146 (1995).
23. Y. Fu and S. L. Jacques, "Monte Carlo simulation for light propagation in 3D tooth model," *Proc. SPIE* **7897**, 78971N (2011).
24. I. Gkigkitzis, "Mathematical modeling of oxygen transport, cell killing and cell decision making in photodynamic therapy of cancer," October 2012, http://thescholarship.ecu.edu/handle/10342/4093 (30 August 2013).
25. T. J. Farrell et al., "Modeling of photosensitizer fluorescence emission and photobleaching for photodynamic therapy dosimetry," *Appl. Opt.* **37**(31), 7168–7183, (1998).
26. R. M. Valentine et al., "Monte Carlo modeling of in vivo protoporphyrin IX fluorescence and singlet oxygen production during photodynamic therapy for patients presenting with superficial basal cell carcinomas," *J. Biomed. Opt.* **16**(4), 048002 (2011).
27. I. Gkigkitzis et al., "Modeling of oxygen transport and cell killing in type-II photodynamic therapy," *Photochem. Photobiol.* **88**(4), 969–977 (2012).
28. M. Kress et al., "Time-resolved microspectrofluorometry and fluorescence lifetime imaging of photosensitizers using picosecond pulsed diode lasers in laser scanning microscopes," *J. Biomed. Opt.* **8**(1), 26–32, (2003).
29. M. Niedre, M. S. Patterson, and B. C. Wilson, "Direct near-infrared luminescence detection of singlet oxygen generated by photodynamic therapy in cells in vitro and tissues in vivo," *Photochem. Photobiol.* **75**(4), 382–391, (2002).
30. I. Georgakoudi et al., "The mechanism of photofrin photobleaching and its consequences for photodynamic dosimetry," *Photochem. Photobiol.* **65**(1), 135–144, (1997).
31. L. Lilge and B. C. Wilson, "Photodynamic therapy of intracranial tissues: a preclinical comparative study of four different photosensitizers," *J. Clini. Laser Med. Surg.* **16**(2), 81–91, (1998).
32. J. D. Vollet-Filho et al., "Possibility for a full optical determination of photodynamic therapy outcome," *J. Appl. Phys.* **105**(10), 102038–102038-7, (2009).

33. B. C. Wilson, M. S. Patterson, and D. M. Burns, "Effect of photosensitizer concentration in tissue on the penetration depth of photoactivating light," *Laser. Med. Sci.* **1**(4), 235–244, (1986).

Lisa Bürgermeister is a research associate at Fraunhofer ILT in Aachen and is working on her dissertation in modeling and simulation of laser medical applications there. She studied physics at RWTH Aachen University and UPMC Paris and graduated in September 2010 with her diploma thesis in the Department of Nonlinear Dynamics of Laser Processing at RWTH Aachen University. Her research interests include modeling and simulation of reaction diffusion systems in medical applications and laser processing.

Fernando Romero López has studied physics at the University of Valencia since 2011. He is now an exchange student at the University of Bonn, Germany. He has been working at Fraunhofer ILT since July 2013, first as a trainee with a DAAD scholarship and currently as a student assistant.

Wolfgang Schulz studied physics in Braunschweig University of Technology. He graduated in theoretical physics in 1985. In 1987, he came to the Department of Laser Technology at RWTH Aachen University and joined later Fraunhofer ILT in Aachen. Since 2005, he has represented the Department of Nonlinear Dynamics of Laser Processing at RWTH Aachen University and is the head of the Department of Modelling and Simulation at the Fraunhofer ILT.